Optimal photon-pair single mode coupling in narrow-band spontaneous parametric down-conversion with arbitrary pump profile

Jean-Loup Smirr,[1] Matthieu Deconinck,[1] Robert Frey,[1] Imad Agha,[1] Eleni Diamanti,[1] and Isabelle Zaquine[1,*]

[1] *Institut TELECOM/Telecom ParisTech – CNRS/LTCI*
46 rue Barrault 75013 PARIS, *France*

(Dated: 2012)

A theoretical investigation of the performance of single-mode coupled spontaneous parametric down-conversion sources is proposed, which only requires very few assumptions of practical interest: quasi-degenerate collinear generation and narrow bandwidth obtained through spectral filtering. Other assumptions like pump beam spatial and temporal envelopes, target single-mode profile and size, and non-linear susceptibility distribution, are only taken into account in the final step of the computation, thus making the theory general and flexible. Figures of merit for performance include absolute coupled brightness and conditional coupling efficiency. Their optimization is investigated using functions that only depend on dimensionless parameters, so that the results provide the best experimental configuration for a whole range of design choices (e.g. crystal length, pump power). A particular application of the theory is validated by an experimental optimization obtained under compatible assumptions. A comparison with other works and proposals for numerically implementing the theory under less stringent assumptions are also provided.

OCIS codes: 270.5565, 190.4410, 270.5290, 060.2330.

1. Introduction

Sources of entangled photons have applications ranging from fundamental tests of quantum mechanics [1, 2] to quantum information and communications [3, 4]. Entanglement based quantum key distribution protocols have been reported [5] as an alternative to those based on single photon sources and quantum repeaters have also been shown to require entanglement as a primary resource [6, 7].

Spontaneous parametric down-conversion (SPDC) remains the simplest way to generate entangled photons, enabling telecommunication wavelength generation which cannot be easily achieved using atomic cascades. A large choice of configurations is available according to the emission geometry (collinear [8] or not [9, 10]), the phase matching type (I [11] or II [9]) and the signal and idler frequencies (degenerate [12] or not [13]). The non-collinear emission geometry has some advantages, providing direct separation of signal and idler photons but collinear emission in periodically poled crystals recently became increasingly popular [14–16], because of the high brightness obtained with longer crystals and higher non-linear susceptibilities.

Filtering is one of the most important aspects of photon pair engineering. Spatial filtering and more specifically coupling the photon pairs to a single spatial mode, like an optical fiber, is the first requirement for long-distance communications. The coupling efficiency is then a crucial parameter, knowing that photon losses limit the visibility of quantum interferences [17, 18]. Narrowband spectral filtering can be necessary to ensure spectral indistinguishability but also to obtain efficient coupling to a quantum memory [19–23] which is a central element in quantum repeaters [3, 20]. It is also beneficial for long-distance communications of polarization states as it reduces polarization mode dispersion and group delay dispersion problems.

Since the pioneering works of SPDC concerning the quantum fluctuation and noise in parametric processes [24] and those dealing with probability of coincidences in the emission of signal and idler photons [25–27] an important theoretical effort has been developed in order to optimize various kind of sources [28, 29], some of them dedicated to strongly focused beams [30].

After studies of the collection of SPDC through apertures [31, 32], numerous authors have reported studies of the coupling of SPDC into a single spatial mode like that of a fiber [33–39], with various assumptions and experimental methods of validation. The optimal focusing of a continuous wave monochromatic pump has been investigated [36] in order to calculate the maximum coupling efficiency of photon pairs into single-mode fibers but the pump diffraction was neglected and the phase mismatch was not taken into account in the optimization process. The same approximations have been used in [37] to calculate the absolute emission rates of SPDC into single modes, where the crystal is moreover assumed to be thin.

*Corresponding author: isabelle.zaquine@telecom-paristech.fr

The absolute coupled brightness is also calculated in [38] but with a continuous wave pump, emphasizing the parallel between SPDC and classical nonlinear phenomena. Very recently, R. S. Bennink studied the case of Gaussian beam profiles, directly writing the nonlinear interaction Hamiltonian with a Gaussian beam profile for both the pump and the SPDC generated photon pairs [39]. This method enables the evaluation of the coupled brightness in a Gaussian target mode and can be adapted to include the effect of spectral filtering; it therefore leads to interesting results that are complementary to ours.

To our knowledge, a comprehensive study of narrowband SPDC pumped by a diffracting beam of arbitrary pulse envelope and duration (from short pulses to continuous-wave lasers) and arbitrary transverse profile, covering a full range of focusing (from tight focusing to parallel beams) and arbitrary filter shapes, has not been addressed. Such a generalization can however be useful in view of optimizing future SPDC sources that might require specific spectral and spatial characteristics to interface with particular quantum information systems.

In this paper, we propose a theoretical framework that is general enough to allow the investigation of these characteristics and their effects on the source performance (e.g. coupled brightness, conditional coupling efficiency) under assumptions suited to the desirable features mentioned above: narrow-bandwidth and collinear emission in long crystals with a given non-linear susceptibility distribution. Using a dedicated source, we also experimentally validate the theoretical predictions for particular assumptions.

Section 2 describes the general formalism of the addressed problem and derives the wave-function of the created photon pairs, taking into account spatial and spectral filtering. We also define various figures of merit that are useful to characterize a source performance. The numerical application of this general theoretical approach to the case of a narrowband fibered source pumped by a Gaussian beam is developed in section 3. The experimental setup is described in section 4 and the measured performances are compared with the theoretical predictions. A comparison of our results with other works, as well as guidelines for generalizing the numerical calculations are proposed in section 5.

2. Theoretical framework

A. The down-converted two-photon state

The general configuration considered hereafter is depicted in Figure 1. The nonlinear interaction takes place in a crystal with a second-order susceptibility $\overline{\overline{\boldsymbol{\chi}}}^{(2)}(\mathbf{r})$, pumped by a classical field of positive-frequency complex amplitude $\mathbf{E}_p^{(+)}$. The spontaneous parametric down-conversion process is described by a time-dependent Hamiltonian $\hat{\mathcal{H}}(t)$. The signal and idler fields $\hat{\mathbf{E}}_s^{(+)}$ and $\hat{\mathbf{E}}_i^{(+)}$ have the following plane-wave decomposition in the

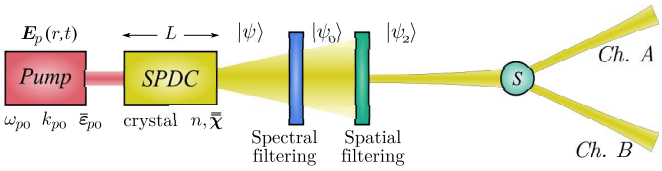

Fig. 1. General configuration considered in the theoretical framework: a nonlinear crystal is pumped by a beam of arbitrary temporal and spatial profiles. The photon pairs produced through SPDC are spectrally filtered and coupled to a single spatial mode, before being split towards channels A and B.

quantization volume $\mathcal{V}$:

$$\hat{\mathbf{E}}_{s,i}^{(+)}(\mathbf{r},t) = \sum_{\ell_{s,i}} \vec{\boldsymbol{\varepsilon}}_{\ell_{s,i}} \hat{a}_{\ell_{s,i}} A(\ell_{s,i}) e^{\mathrm{i}(\mathbf{k}_{\ell_{s,i}}\cdot\mathbf{r} - \omega_{\ell_{s,i}} t)} \tag{1}$$

where the field amplitude $A(\ell)$ for the mode ℓ associated with annihilation operator $\hat{a}_\ell$ is

$$A(\ell) = \mathrm{i}\sqrt{\frac{\hbar\omega_\ell}{2\epsilon_0 \mathcal{V} n^2(\mathbf{k}_\ell)}}. \tag{2}$$

Frequency and polarization are respectively denoted by ω_ℓ and $\vec{\boldsymbol{\varepsilon}}_\ell$, wavevectors in the crystal by $\mathbf{k}_\ell$. A notation $\mathbf{k}'_\ell$ will be used when the wavevector is evaluated in another medium.

In the interaction picture, the Hamiltonian is given by [40, 41]

$$\hat{\mathcal{H}}(t) = \epsilon_0 \int d^3\mathbf{r}\, \mathbf{E}_p^{(+)}(\mathbf{r},t)\, \overline{\overline{\boldsymbol{\chi}}}^{(2)}(\mathbf{r}) \hat{\mathbf{E}}_s^{(-)}(\mathbf{r},t) \hat{\mathbf{E}}_i^{(-)}(\mathbf{r},t) + H.c. \tag{3}$$

where $\hat{\mathbf{E}}^{(-)}$ is the Hermitian conjugate ($H.c.$) of $\hat{\mathbf{E}}^{(+)}$.

The pump field is assumed to be a linearly $\vec{\boldsymbol{\varepsilon}}_x$-polarized classical paraxial beam propagating along the z axis with L^2-normalized temporal and spatial envelopes T_p and S_p.

Using transverse coordinates $\boldsymbol{\rho} = \binom{x}{y}$ such that $\mathbf{r} = \binom{\boldsymbol{\rho}}{z}$,

$$\mathbf{E}_p^{(+)}(\boldsymbol{\rho},z,t) = \vec{\boldsymbol{\varepsilon}}_x C_p T_p\Big(t - \frac{z}{v_p}\Big) S_p(\boldsymbol{\rho},z) e^{\mathrm{i}(k_{p_0} z - \omega_{p_0} t)}. \tag{4}$$

Here k_{p_0} is the pump wavevector modulus at its central frequency ω_{p_0} and v_p is the group velocity in the crystal. We neglect its spectral dispersion, therefore $v_p = c/n_p$ where n_p is the refractive index in the crystal at ω_{p_0}. The constant $C_p = \sqrt{\mathscr{E}_p/(2\epsilon_0 n_p^2 v_p)}$ depends on the pump pulse energy $\mathscr{E}_p$.

When the down-conversion efficiency is small, the generated two-photon state is the first-order approximate solution to the Schrödinger equation. Discarding the zeroth-order term,

$$|\psi(t)\rangle = \frac{1}{\mathrm{i}\hbar}\int_{-\infty}^{t} dt' \hat{\mathcal{H}}(t')|0\rangle. \tag{5}$$

Let us separate the spatial dependence $R(\mathbf{r})$ of the nonlinear susceptibility:

$$\vec{\varepsilon}_x\,\overline{\overline{\chi}}^{(2)}(\mathbf{r})\vec{\varepsilon}_{\ell_s}\vec{\varepsilon}_{\ell_i} = \chi(\ell_s,\ell_i)\cdot R(\mathbf{r}). \tag{6}$$

After the pump has propagated through the whole crystal length, ($t\to\infty$), the state is time-independent in the interaction picture. Identifying the integral in Eq. (5) as the Fourier transform $\breve{E}_p^{(+)}$ of $\mathbf{E}_p^{(+)}\cdot\vec{\varepsilon}_x$ with respect to its temporal variable, the state is given by

$$|\psi\rangle = \frac{\epsilon_0}{\mathrm{i}\hbar}\sum_{\ell_s,\ell_i}\chi(\ell_s,\ell_i)A(\ell_s)A(\ell_i)\int d^3\mathbf{r}\, e^{-\mathrm{i}(\mathbf{k}_{\ell_s}+\mathbf{k}_{\ell_i})\cdot\mathbf{r}} \times R(\mathbf{r})\breve{E}_p^{(+)}(\mathbf{r},\omega_{\ell_s}+\omega_{\ell_i})\hat{a}^\dagger_{\ell_s}\hat{a}^\dagger_{\ell_i}|0\rangle \tag{7}$$

This equation can be understood as the sum of the contributions of local interactions to the delocalized down-converted two-photon state $|\psi\rangle$. The integral has the form of a spatial Fourier transform, which leads to

$$|\psi\rangle = \sum_{\ell_s,\ell_i}\gamma_0(\ell_s,\ell_i)\hat{a}^\dagger_{\ell_s}\hat{a}^\dagger_{\ell_i}|0\rangle \tag{8}$$

where

$$\gamma_0(\ell_s,\ell_i) = \frac{\epsilon_0}{\mathrm{i}\hbar}\chi(\ell_s,\ell_i)A(\ell_s)A(\ell_i) \times \breve{R}*\breve{E}_p^{(+)}(\mathbf{k}_{\ell_s}+\mathbf{k}_{\ell_i},\omega_{\ell_s}+\omega_{\ell_i}) \tag{9}$$

$\breve{R}$ being the Fourier transform of R and $*$ the convolution operator. Using the fact that, for a diffracting beam in the paraxial approximation, the Fourier transform of the transverse spatial envelope has the following z dependence:

$$\breve{S}_p(\boldsymbol{\kappa},z) = \breve{S}_p(\boldsymbol{\kappa},0)e^{-\mathrm{i}\frac{|\boldsymbol{\kappa}|^2}{2k_{p_0}}z} \tag{10}$$

where $\boldsymbol{\kappa}$ is the transverse wavevector, we have

$$\breve{E}_p^{(+)}(\boldsymbol{\kappa},k_z,\omega) = C_p\breve{T}_p(\omega-\omega_{p_0})\breve{S}_p(\boldsymbol{\kappa},0) \times 2\pi\delta\big(k_z-k_{p_0}-\frac{\omega-\omega_{p_0}}{v_p}+\frac{|\boldsymbol{\kappa}|^2}{2k_{p_0}}\big). \tag{11}$$

We consider a crystal of length L centered on $z=0$ whose transverse dimensions are large compared to the pump beam profile. If its nonlinear susceptiblity distribution is transversally invariant, it can be expressed as a one-dimensional Fourier series:

$$R(z) = \mathrm{rect}(z/L)\times\sum_m R_m e^{-\mathrm{i}2\pi m\frac{z}{L}} \tag{12}$$

where $\mathrm{rect}(z)$ is the rectangular function with $\mathrm{rect}(0)=1$. In the reciprocal space,

$$\breve{R}(k_z) = \sum_m R_m\,\mathrm{sinc}\,(k_z+2\pi m/L)\,. \tag{13}$$

Then $\gamma_0(\ell_s,\ell_i)=\sum_m\gamma_{0m}(\ell_s,\ell_i)$ with

$$\gamma_{0m}(\ell_s,\ell_i) = \frac{\epsilon_0}{\mathrm{i}\hbar}R_m\chi(\ell_s,\ell_i)A(\ell_s)A(\ell_i) \times C_p\breve{T}_p(\omega_{\ell_s}+\omega_{\ell_i}-\omega_{p_0})\breve{S}_p(\boldsymbol{\kappa}_{\ell_s}+\boldsymbol{\kappa}_{\ell_i},0) \times L\,\mathrm{sinc}\left(\Delta K_m(\mathbf{k}_{\ell_s}+\mathbf{k}_{\ell_i},\omega_{\ell_s}+\omega_{\ell_i})\frac{L}{2}\right) \tag{14}$$

where

$$\Delta K_m(\mathbf{k},\omega) = k_z - k_{p_0} - \frac{\omega-\omega_{p_0}}{v_p} + \frac{|\boldsymbol{\kappa}|^2}{2k_{p_0}} + m\frac{2\pi}{L}. \tag{15}$$

So far, we have written explicitly in Eq. (8) the unnormalized state, $|\psi\rangle$, of a photon-pair down-converted during a pump pulse. Its squared modulus $\langle\psi|\psi\rangle$ is the probability that such a down-conversion effectively occurs. The effect of spectral and spatial filtering on the photon-pair state is developed in the following section.

B. Spectral and spatial filtering

The calculation of the effect of filtering on one-photon states is detailed in Appendix A. Extrapolation to two-photon states is straightforward and only results are given here. Filters give rise to losses and two photon states are consequently transformed into mixed states, i.e. non coherent superpositions of two-photon, one-photon and zero-photon terms. In the case of coincidence counting, the two-photon state component is post-selected and we will discard zero- and one-photon terms.

Purely spectral filters are described by a function $\mathcal{F}(\omega-\omega_\mathrm{F})$ defining their amplitude transmission with a maximum normalized at 1 at their central frequency ω_F. More generally, a spectral filter can be sensitive to the direction of the wavevector (like prisms, gratings or Fabry-Pérot etalons), and it may be necessary to take a $\boldsymbol{\kappa}$-dependence into account: $\mathcal{F}(\omega-\omega_\mathrm{F},\boldsymbol{\kappa})$.

Spatial filtering is modeled as the coupling of the down-converted field to a single spatial mode defined, in a medium of refractive index n', by a frequency dependent function $\mathcal{O}_{\omega,0}(\mathbf{r})$. The filter location $z=z_0$ defines the transverse plane where the coupling is considered to take place. This coupling induces a state projection on the target mode, and the state of the transmitted photons is associated to a creation operator $\hat{o}^\dagger_\omega$.

Following Eq. (8), the spectrally-filtered, free-space two-photon state is given by

$$|\psi_0\rangle = \sum_{\ell_s,\ell_i}\gamma_0(\ell_s,\ell_i)\gamma_T^{(2)}(\ell_s,\ell_i)\hat{a}^\dagger_{\ell_s}\hat{a}^\dagger_{\ell_i}|0\rangle \oplus \textit{ignored one and zero-photon terms.} \tag{16}$$

where $\oplus$ stands for the incoherent sum of components of a statistical mixture (see also end of Appendix A) and

$$\gamma_T^{(2)}(\ell_s,\ell_i) = \mathcal{F}(\omega_{\ell_s}-\omega_{s_0},\boldsymbol{\kappa}_{\ell_s})\mathcal{F}(\omega_{\ell_i}-\omega_{i_0},\boldsymbol{\kappa}_{\ell_i}), \tag{17}$$

ω_{s_0} and ω_{i_0} being the signal and idler frequencies selected by the filters, which can be equal for degenerate down-conversion using a unique filter. The squared modulus of this state, $\langle\psi_0|\psi_0\rangle$, is the probability P_0 of generating a photon pair during a pump pulse in the filter bandwidth.

The spectrally and spatially filtered state is given by

$$|\psi_2\rangle = \sum_{\ell_s,\ell_i} \gamma_0(\ell_s,\ell_i)\gamma_T^{(2)}(\ell_s,\ell_i)\gamma_S^{(2)}(\ell_s,\ell_i)\hat{o}^\dagger_{\omega_{\ell_s}}\hat{o}^\dagger_{\omega_{\ell_i}}|0\rangle \\ \oplus \textit{ ignored one and zero-photon terms.} \quad (18)$$

with

$$\gamma_S^{(2)}(\ell_s,\ell_i) = \frac{1}{\mathcal{S}}\breve{\mathcal{O}}^*_{\omega_{\ell_s},0}(\boldsymbol{\kappa}_{\ell_s},z_0)\breve{\mathcal{O}}^*_{\omega_{\ell_i},0}(\boldsymbol{\kappa}_{\ell_i},z_0) \\ \times e^{\mathrm{i}(k'_{z,\ell_s}+k'_{z,\ell_i})z_0} \quad (19)$$

where $\breve{\mathcal{O}}^*_{\omega,0}$ is the complex conjugate of the transverse Fourier transform of $\mathcal{O}_{\omega,0}$, $k'_{z,\ell} = k_{z,\ell}n'(\omega_\ell)/n(\omega_\ell)$ is the longitudinal wavevector evaluated in a medium of refractive index n', and $\mathcal{S}$ is the transverse section of the quantization volume (see Appendix A for details).

After spectral and spatial filtering, $|\psi\rangle$ has become $|\psi_2\rangle$. Since the state has not been renormalized, $P_2 = \langle\psi_2|\psi_2\rangle$ is the probability that one pulse has generated a photon pair and that this pair has been transmitted by the spectral and spatial filters. Its calculation is performed in subsection 2 D, using assumptions that will allow us to separate the frequency dependence from the wavevector dependence in Eq. (15) as shown in the next subsection.

C. *Assumptions*

A few assumptions are quite natural when aiming at applications in quantum information. Moreover, they enable further analytical development as well as faster numerical calculation. The following approximations, mostly used to simplify the expressions of ΔK in (19), aim at eventually decoupling the frequency dependence (ω) from the angular dependence ($\boldsymbol{\kappa}$) in the wavevectors $\mathbf{k}$.

1. Collinear collection

When using long crystals, as in most recent and efficient devices [42, 43], a collinear configuration is required. In such a case, the paraxial approximation, as already used for the pump beam, can be applied to the down-converted photons on the z-axis, giving the following expression for the longitudinal component of the signal wavevector:

$$k_{z\,s} = k_{s_0} + \frac{\omega_s - \omega_{s_0}}{v_s} - \frac{1}{2}\frac{|\boldsymbol{\kappa}_s|^2}{|\mathbf{k}_s|} \quad (20)$$

where k_{s_0} is the wavenumber of collinearly emitted signal photons at the central frequency of the filter ω_{s_0}, and $v_s = c/n_s$ with n_s the refractive index in the crystal at the signal frequency. A similar expression applies for $k_{z\,i}$.

2. Narrow bandwidth

When filtering limits the source bandwidth to less than a few nanometers ($\Delta\omega_\mathrm{F} \ll \omega_{p_0}$), we have $\omega_s \approx \omega_{s_0}$ and $\omega_i \approx \omega_{i_0}$ in which case, according to Eq. (20), the phase mismatch ΔK depends only on $\boldsymbol{\kappa}_s, \boldsymbol{\kappa}_i$. The field amplitudes and nonlinear susceptibility, respectively defined in Eqs. (2) and (6), can then be considered constant. In quantum memories based on atomic and ionic resonances, the acceptance bandwidth is lower than a few GHz [22], which definitely lies within the present assumption.

3. Spatial dependence of the nonlinear susceptibility

Although it is possible to calculate $\sum_m \gamma_{0m}$ for an arbitrary $R(z)$, this function is generally chosen such that one term $\gamma_{0\tilde{m}}$ is as high as possible and is the only optimally phase-matched one. This is achieved by periodically poling the nonlinear susceptibility with a period Λ. In this case, $\tilde{m}$ should be chosen such that $L = \tilde{m}\Lambda$, and $R_{\tilde{m}} = 2/\pi$ is the first term of the Fourier expansion of a square periodic function. In the following, we will consider the case of a collinear interaction in a periodically poled crystal with an effective susceptibility $\chi_\mathrm{eff} = \chi(\omega_{s_0},\omega_{i_0}) \times 2/\pi$ corresponding to specific polarizations of the pump, signal and idler beams. The case of the homogeneous crystal could also be described using an infinite period and $R_{\tilde{m}} = 1$.

4. Quasi-degenerate down-conversion

In the following, we will restrict the process to quasi-degenerate down-conversion, that is $|\delta\omega| \ll \omega_{p_0}$ with $\delta\omega = \omega_{s_0} - \omega_{i_0}$.

The phase mismatch then reduces to

$$\Delta K(\boldsymbol{\kappa}_s,\boldsymbol{\kappa}_i) \approx \Delta k_0 + \frac{|\boldsymbol{\kappa}_s+\boldsymbol{\kappa}_i|^2}{2k_{p_0}} \\ - \Big(1-\frac{\delta\omega}{\omega_{p_0}}\Big)\frac{n_p}{n_s}\frac{|\boldsymbol{\kappa}_s|^2}{k_{p_0}} - \Big(1+\frac{\delta\omega}{\omega_{p_0}}\Big)\frac{n_p}{n_i}\frac{|\boldsymbol{\kappa}_i|^2}{k_{p_0}} \quad (21)$$

where $\Delta k_0 = k_{s_0} + k_{i_0} - k_{p_0} + \frac{2\pi}{\Lambda}$ is the longitudinal phase mismatch. This together with the narrow bandwidth assumption allows to omit the frequency dependence of the functions $\mathcal{O}_{\omega,0}$ describing the target mode. It can therefore be replaced by the unique function $\mathcal{O}_0 = \mathcal{O}_{\omega_{p_0}/2,0} \approx \mathcal{O}_{\omega_{s_0},0} \approx \mathcal{O}_{\omega_{i_0},0}$.

D. *Figures of merit*

In our general configuration of Fig. 1, only the photon pairs that are spectrally and spatially filtered, with a probability P_2, will give rise to measured coincidences between the two channels: P_2 will be called *coupled brightness*. The source coherence can be quantified by the ratio of coincidences to single counts. In our framework this is directly related to the probability $\Gamma_{2|1}$ of having the idler photon coupled to the target spatial mode when the signal is coupled to that mode (or vice versa). Sometimes called *conditional coupling efficiency*, this parameter is very useful as a quality figure of merit when the source is to be used as an entangled photon pair source. It will

be evaluated using the single-photon coupling probability P_1 of having at least one photon transmitted by the filters. In the following subsections, a detailed calculation of each of these parameters is given.

1. Coupled brightness

The coincidental presence of both photons in the target spatial mode over a whole pulse duration is based on the two-photon state $|\psi_2\rangle$ (Eq. (18)) and is given by

$$P_2 = \langle\psi_2|\psi_2\rangle \tag{22}$$

To make further calculations, we take the limit of an infinite quantization volume, in which sums over modes ℓ are replaced by integrals over the wavevectors $\mathbf{k}$ in the usual way [44, 45] with discrete variables like $\mathbf{k}_\ell$, ω_ℓ and operators like $\hat{o}_{\omega_\ell}$ changed into their continuous counterparts $\mathbf{k}$, $\omega(\mathbf{k})$ and $\hat{o}(\omega(\mathbf{k}))$. Moreover, the narrow bandwidth assumption allows to calculate integrals over $\boldsymbol{\kappa}$ independently of integrals over ω, since $\boldsymbol{\kappa}$ mostly varies with the wavevector angle when ω is restricted to a small interval. Equation (22) gives, under the previous assumptions:

$$P_2 = |C|^2 \Omega_2 K_2, \tag{23}$$

where

$$C = \mathrm{i} e^{\mathrm{i}(n'_s\omega_{s_0}+n'_i\omega_{i_0})z_0/c}\sqrt{\frac{\mathscr{E}_p\chi^2_{\mathrm{eff}}\omega_{s_0}\omega_{i_0}}{8\epsilon_0 c^3 n_p n_s n_i}} \tag{24}$$

is a constant with n'_s (resp. n'_i) the refractive index in the medium.

Using the target mode $\mathcal{O}_0$ introduced in subsection 2 C 4, the functions

$$\Omega_2 = \int\frac{d\omega_s}{2\pi}\int\frac{d\omega_i}{2\pi}\left|\breve{T}_p(\omega_s+\omega_i-\omega_{p_0}) \times \mathcal{F}(\omega_s-\omega_{s_0})\mathcal{F}(\omega_i-\omega_{i_0})\right|^2 \tag{25}$$

and

$$K_2 = \left|\iint\frac{d^2\boldsymbol{\kappa}_s}{(2\pi)^2}\iint\frac{d^2\boldsymbol{\kappa}_i}{(2\pi)^2}\breve{S}_p(\boldsymbol{\kappa}_s+\boldsymbol{\kappa}_i,0) \times \breve{\mathcal{O}}_0(\boldsymbol{\kappa}_s,z_0)\breve{\mathcal{O}}_0(\boldsymbol{\kappa}_i,z_0)e^{-\mathrm{i}z_0\left(\frac{n_p}{n'_s}\frac{|\boldsymbol{\kappa}_s|^2}{k_{p_0}}+\frac{n_p}{n'_i}\frac{|\boldsymbol{\kappa}_i|^2}{k_{p_0}}\right)} \times L\,\mathrm{sinc}\left(\frac{\Delta K(\boldsymbol{\kappa}_s,\boldsymbol{\kappa}_i)\,L}{2}\right)\right|^2 \tag{26}$$

describe respectively the spectral and spatial dependence of P_2. They must be both maximized in order to optimize the coupled brightness.

The function Ω_2 has the dimension of a frequency and can be interpreted as the effective source bandwidth. It can be written as a convolution of the three spectrally-dependent functions and, as such, it is maximum when the filters are tuned so as to satisfy the energy conservation $\omega_{s_0}+\omega_{i_0}=\omega_{p_0}$:

$$\Omega_2 = |\breve{T}_p|^2 * |\mathcal{F}|^2 * |\mathcal{F}|^2(\omega_{s_0}+\omega_{i_0}-\omega_{p_0}) \tag{27}$$

In the following, we will assume that this energy conservation condition is satisfied.

The dimensionless function K_2 takes into account the spatial interferences caused both by phase matching and coupling to the target mode. Its maximization will require a numerical optimization (see 3 C 2).

The factor $|C|^2$ appears then as a spectral probability density.

2. Conditional coupling efficiency

Evaluating the conditional coupling efficiency requires calculating the single-photon coupling probability defined by

$$P_1 = \langle\psi_1|\psi_1\rangle \tag{28}$$

for the state

$$|\psi_1\rangle = \sum_{\ell_s,\ell_i}\gamma_0(\ell_s,\ell_i)\gamma_T^{(1)}(\ell_s)\gamma_S^{(1)}(\ell_s)\hat{o}^\dagger_{\omega_{\ell_s}}\hat{a}^\dagger_{\ell_i}|0\rangle \oplus \textit{ignored zero-photon terms} \tag{29}$$

where

$$\gamma_T^{(1)} = \mathcal{F}(\omega_{\ell_s}-\omega_{s_0},\boldsymbol{\kappa}_{\ell_s}) \tag{30}$$

corresponds to a spectral filtering of the signal and no filtering for the idler [1], and

$$\gamma_S^{(1)} = \frac{1}{\sqrt{\mathcal{S}}}\breve{\mathcal{O}}_0^*(\boldsymbol{\kappa}_{\ell_s},z_0)e^{\mathrm{i}k'_{z,\ell_s}z_0} \tag{31}$$

describes the coupling of the signal photon only into the target single mode.

In the same way as for P_2,

$$P_1 = |C|^2\Omega_1 K_1 \tag{32}$$

where

$$\Omega_1 = \int\frac{d\omega_s}{2\pi}\int\frac{d\omega_i}{2\pi}\left|\breve{T}_p(\omega_s+\omega_i-\omega_{p_0})\mathcal{F}(\omega_s-\omega_{s_0})\right|^2 \tag{33}$$

$$K_1 = \iint\frac{d^2\boldsymbol{\kappa}_i}{(2\pi)^2}\left|\iint\frac{d^2\boldsymbol{\kappa}_s}{(2\pi)^2}\breve{S}_p(\boldsymbol{\kappa}_s+\boldsymbol{\kappa}_i,0)\breve{\mathcal{O}}_0(\boldsymbol{\kappa}_s,z_0) \times e^{-\mathrm{i}z_0\frac{n_p}{n'_s}\frac{|\boldsymbol{\kappa}_s|^2}{k_{p_0}}}L\,\mathrm{sinc}\,\frac{\Delta K\,L}{2}\right|^2. \tag{34}$$

As K_2, K_1 requires numerical computation, whereas Ω_1 reduces to

$$\Omega_1 = \int\frac{d\omega}{2\pi}|\mathcal{F}(\omega)|^2 \tag{35}$$

which is proportional to the filter bandwidth itself.

[1] The natural phase matching bandwidth has no influence on the results that follow if it is much larger than the pump linewidth.

The conditional coupling efficiency i.e. the conditional probability to couple the second photon to the target spatial mode when its twin has been coupled, is defined by

$$\Gamma_{2|1} = \frac{K_2}{K_1}. \tag{36}$$

Note that the conditional coupling efficiency should not be confused with the heralding ratio, which is often used to refer to the conditional probability to detect one photon when the other one has been detected and includes spectral filtering effects. Notwithstanding trivial factors like detector sensitivities, the heralding ratio is equal to $\frac{P_2}{P_1} = \frac{K_2}{K_1}\frac{\Omega_2}{\Omega_1}$, hence it indeed takes the spectral as well as spatial loss of coherence into account. Since in the narrowband regime spatial and spectral filtering effects can be treated separately, we focus hereafter on optimizing the conditional coupling efficiency independently of spectral factors. Note that in the context of quantum information applications, the complex spectral filtering required, for instance, for quantum memories associated with their limited storage-retrieval efficiency, makes the coupling efficiency a parameter that has to be maximized. Spectral factors are shortly analyzed in subsection 3 C 1; for an indepth investigation of the influence of spectral filtering we refer to our previous work [18, 46].

In order to get a physical insight into these results and show how this description can be used as a tool for the design and optimization of entangled photon pair sources, the following section is devoted to a numerical calculation corresponding to the particular case of the experiment described subsequently in Section 4.

3. Numerical optimization of a narrow-band fibered source pumped by a Gaussian beam

A. *Gaussian pump beam, Gaussian target mode*

We assume the pump beam to be Gaussian with a waist radius w_0 and Rayleigh length z_R:

$$S_p(\boldsymbol{\rho}, 0) = \sqrt{\frac{2}{\pi w_0^2}}\, e^{-|\boldsymbol{\rho}|^2/w_0^2} \tag{37}$$

$$\breve{S}_p(\boldsymbol{\kappa}, 0) = \sqrt{2\pi w_0^2}\, e^{-|\boldsymbol{\kappa}|^2 w_0^2/4} \tag{38}$$

Using the fact that $k_{p_0}/2 = z_R/w_0^2$, the phase matching function from Eq. 21 becomes

$$\Delta K \approx \Delta k_0 + \frac{w_0^2}{4z_R}\Big[|\boldsymbol{\kappa}_s + \boldsymbol{\kappa}_i|^2 - 2\Big(1 - \frac{\delta\omega}{\omega_{p_0}}\Big)\frac{n_p}{n_s}|\boldsymbol{\kappa}_s|^2 - 2\Big(1 + \frac{\delta\omega}{\omega_{p_0}}\Big)\frac{n_p}{n_i}|\boldsymbol{\kappa}_i|^2\Big] \tag{39}$$

The target mode acting as a spatial filter is defined by the profile of a Gaussian mode at its waist of radius a_0 located at z_0. This can be the transverse mode of a fiber or its image by a lens collection system:

$$\mathcal{O}_0(\boldsymbol{\rho}, z_0) = \sqrt{\frac{2}{\pi a_0^2}}\, e^{-|\boldsymbol{\rho}|^2/a_0^2} \tag{40}$$

$$\breve{\mathcal{O}}_0(\boldsymbol{\kappa}, z_0) = \sqrt{2\pi a_0^2}\, e^{-|\boldsymbol{\kappa}|^2 a_0^2/4}. \tag{41}$$

B. *Nondimensionalization*

The coupled brightness P_2 given by Eq. (23) can now be detailed. It is useful to separate the fixed parameters from the configuration of the experiment that can be optimized:

$$P_2 = \frac{\mathscr{E}_p \chi_{\text{eff}}^2 L \Delta\omega_{\text{F}} \omega_{s_0}\omega_{i_0}\omega_{p_0}}{8\epsilon_0 c^4 n_s n_i} \cdot \frac{\Omega_2}{\Delta\omega_{\text{F}}}(\delta) \cdot \frac{K_2}{k_{p_0} L}(\xi, \alpha, \zeta, \varphi_0) \tag{42}$$

where $\Delta\omega_{\text{F}}$ is the filter bandwidth, and the dimensionless spectral and spatial terms $\Omega_2/\Delta\omega_{\text{F}}$ and $K_2/(k_{p_0}L)$ depend only on the experimental configuration described by the following dimensionless parameters:

$$\delta = \frac{4\ln 2}{\Delta t_p \Delta\omega_{\text{F}}} \quad \text{(relative pump bandwidth)}$$

$$\xi = \frac{L}{2z_R} \quad \text{(pump focusing parameter)}$$

$$\alpha = \frac{a_0}{w_0} \quad \text{(normalized target mode waist size)}$$

$$\zeta = \frac{z_0}{L} \quad \text{(longitudinal collection offset)}$$

$$\varphi_0 = \Delta k_0\, L \quad \text{(longitudinal phase mismatch)}$$

$$\boldsymbol{\varphi}_s = \frac{w_0}{2}\boldsymbol{\kappa}_s \quad \text{(normalized signal transverse wavevector)}$$

$$\boldsymbol{\varphi}_i = \frac{w_0}{2}\boldsymbol{\kappa}_i \quad \text{(normalized idler transverse wavevector)}$$

The parameter Δt_p is the pump pulse duration. Eq. (42), that will be used to calculate the conditional coupling efficiency, has a particular importance, as it quantifies the coupled brightness and its dependence on various experimental parameters. It will be discussed and compared to other reported works in section 5. In the following section we will theoretically determine the experimental configuration that maximizes this brightness.

C. *Optimization of the coupled brightness*

1. Spectral optimization

The optimisation of Ω_2 from Eq. (25) must generally be made numerically, but the influence of the relative pump bandwidth δ can be developped in a fully analytical way if the pump temporal envelope and the spectral filters

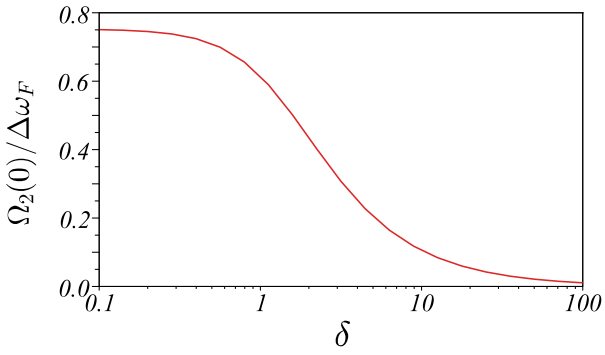

Fig. 2. Effect of the relative Gaussian pump linewidth δ on the spectral transmission factor $\Omega_2/\Delta\omega_{\rm F}$ for Gaussian spectral filters.

are both Gaussian:

$$T_p(t) = \left[\frac{4\ln 2}{\pi\Delta t_p^2}\right]^{\frac{1}{4}} e^{-2\ln 2\, t^2/\Delta t_p^2} \tag{44}$$

$$\breve{T}_p(\omega) = \left[\frac{\pi\Delta t_p^2}{\ln 2}\right]^{\frac{1}{4}} e^{-\omega^2\Delta t_p^2/(8\ln 2)} \tag{45}$$

$$\mathcal{F}(\omega) = e^{-2\ln 2\,\omega^2/\Delta\omega_{\rm F}^2} \tag{46}$$

where Δt_p and $\Delta\omega_{\rm F}$ are full widths at half maximum intensity. The spectral transmission factor can then be expressed as a function of the relative pump bandwidth δ in the following way:

$$\frac{\Omega_2}{\Delta\omega_{\rm F}}(\delta) = \sqrt{\frac{\pi/(8\ln 2)}{1+\frac{\delta^2}{2}}} \tag{47}$$

This quantity is plotted in Fig. 2 showing that the maximum value is asymptotically reached when the pump beam is monochromatic. The joint probability for a photon and its twin to be transmitted is then optimal.

When the pump linewidth increases, some idler photons at $\omega_i = \omega_p - \omega_s$ and their corresponding signal photon at ω_s are not frequency-symmetric with respect to the filter center frequency ($\omega_p \neq \omega_{p_0}$), which is necessarily detrimental. This effect becomes significant as the pump linewidth gets greater than the filter bandwidth ($\delta \geq 1$). As a consequence, even though it could seem beneficial to reduce the pulse duration Δt_p in order to achieve a higher repetition rate, the curve of Fig. 2 shows that it would also contribute to decrease Ω_2. In other words, the achievable photon pair rate per second is a result of a compromise on the pulse duration, which is all the more stringent as the filter bandwidth is low.

2. Spatial optimization for degenerate down-conversion

In the following, we restrict ourselves to the case of a frequency-degenerate down-conversion ($\omega_s = \omega_i$), which corresponds to the experimental setup described in section 4. The dimensionless term to be optimized has the following expression:

$$\frac{K_2}{k_{p_0}L}(\xi,\alpha,\zeta,\varphi_0) = \frac{8}{\pi^5}\xi\alpha^4\Big|\iint d^2\boldsymbol{\varphi}_s \iint d^2\boldsymbol{\varphi}_i\; Q_2\Big|^2 \tag{48}$$

with

$$\begin{aligned} Q_2 = {} & \exp\Big\{-|\boldsymbol{\varphi}_s+\boldsymbol{\varphi}_i|^2\Big\} \\ & \times \exp\Big\{-\alpha^2\big(|\boldsymbol{\varphi}_s|^2+|\boldsymbol{\varphi}_i|^2\big)\Big\} \\ & \times \exp\,\mathrm{i}\Big\{-4\xi\zeta\left(\frac{n_p}{n_s'}|\boldsymbol{\varphi}_s|^2+\frac{n_p}{n_i'}|\boldsymbol{\varphi}_i|^2\right)\Big\} \\ & \times \mathrm{sinc}\left\{\frac{\varphi_0}{2}+\xi\Big[|\boldsymbol{\varphi}_s+\boldsymbol{\varphi}_i|^2-2\frac{n_p}{n_s}|\boldsymbol{\varphi}_s|^2-2\frac{n_p}{n_i}|\boldsymbol{\varphi}_i|^2\Big]\right\} \end{aligned} \tag{49}$$

Using polar coordinates, we can use the following mapping:

$$\begin{aligned} &\iint d^2\boldsymbol{\varphi}_s \iint d^2\boldsymbol{\varphi}_i\; Q_2 \\ &\qquad \longrightarrow 2\pi\int_0^\infty \rho_s d\rho_s \int_0^\infty \rho_i d\rho_i \int_0^{2\pi} d(\theta_s-\theta_i)\; Q_2' \end{aligned} \tag{50}$$

with

$$\begin{aligned} Q_2' = {} & \exp\Big\{-\big(1+\alpha^2\big)\big(\rho_s^2+\rho_i^2\big)\Big\} \\ & \times \exp\Big\{-2\rho_s\rho_i\cos(\theta_s-\theta_i)\Big\} \\ & \times \exp\,\mathrm{i}\Big\{-4\xi\zeta\left(\frac{n_p}{n_s'}\rho_s^2+\frac{n_p}{n_i'}\rho_i^2\right)\Big\} \\ & \times \mathrm{sinc}\left\{\frac{\varphi_0}{2}+\xi\Big[\big(1-2\frac{n_p}{n_s}\big)\rho_s^2+\big(1-2\frac{n_p}{n_s}\big)\rho_i^2 \right. \\ & \qquad \left. +2\rho_s\rho_i\cos(\theta_s-\theta_i)\Big]\right\} \end{aligned} \tag{51}$$

In this way, the quadruple integral turns into a triple integral which is numerically evaluated using an adaptative 3D quadrature algorithm [47].

Figure 3 represents, for three different pump focusing parameters ξ, the value of the spatial filtering term $K_2/(k_{p_0}L)$ as a function of parameters α and φ_0. It shows that there exists a unique couple $(\alpha^{\rm opt}, {\varphi_0}^{\rm opt})$ that allows reaching the maximum $K_2^{\rm opt}/(k_{p_0}L)$ for a given value of ξ. Moreover, that maximum varies with ξ and the accuracy of $(\alpha^{\rm opt}, {\varphi_0}^{\rm opt})$ is found to be more critical for low ξ. Indeed, when the focusing of the pump beam increases, phase matching can only be satisfied in an average way, because of the large range of emitted angles, and $\alpha^{\rm opt}$ results from a compromise between collecting weakly divergent photons with high efficiency and reducing this efficiency to collect more strongly divergent photons. Optimizing the pump beam for photon pair collection indeed consists in finding the focusing parameter for which these two compromises offer the best performance.

Note that in Fig. 3, the normalized longitudinal offset of single-mode collection ζ has been set to zero. We have checked that this choice gives optimal results. The optimality of $\zeta = 0$ is due to the symmetry of the problem

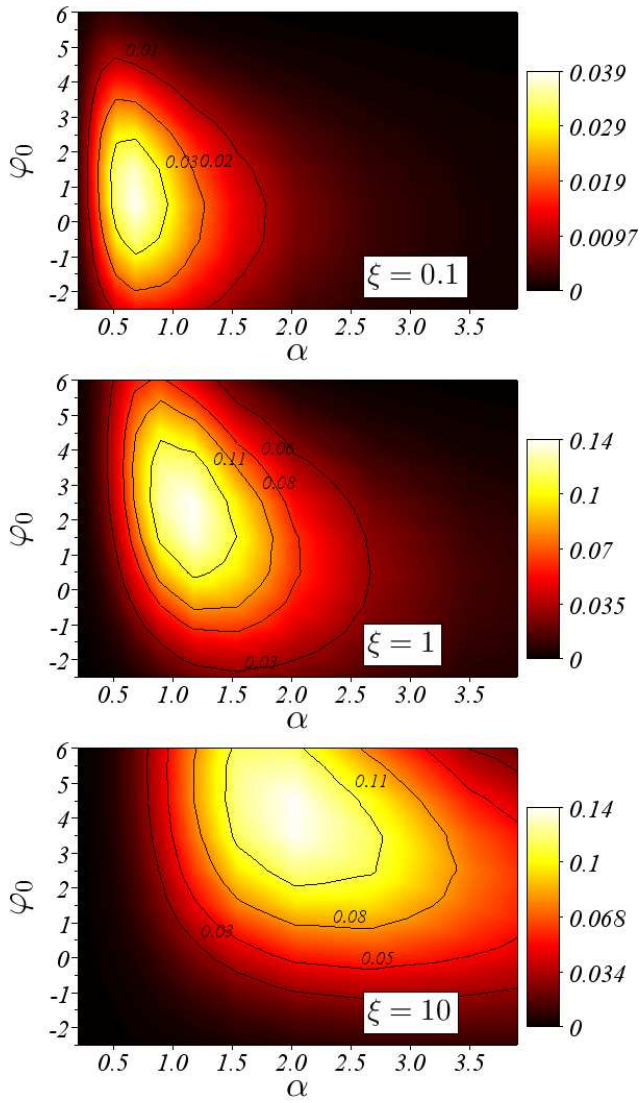

Fig. 3. Optimization of the spatial filtering factor $K_2/(k_{p_0}L)$ with respect to the normalized target mode waist α and the longitudinal phase mismatch φ_0 for three values of the focusing parameter ξ: $\xi = 0.1$ (a), $\xi = 1$ (b) and $\xi = 10$ (c).

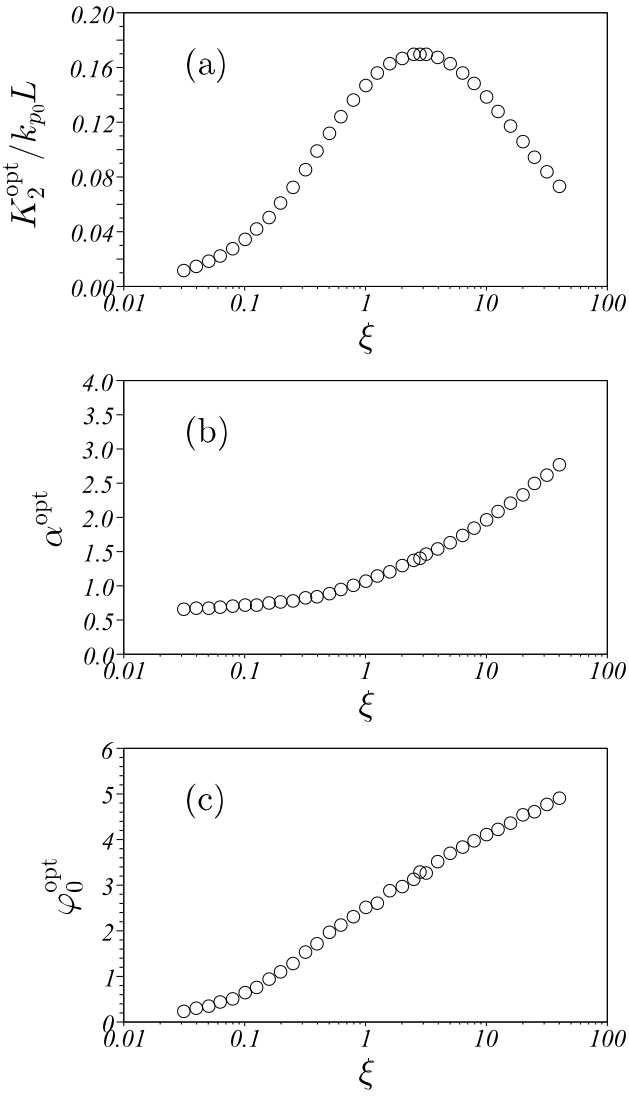

Fig. 4. Maximal value of the spatial filtering factor $K_2/(k_{p_0}L)$ (a) and associated optimal values of the normalized target mode waist α (b) and the longitudinal phase mismatch φ_0 (c), for various values of the focusing parameter ξ.

in our particular choice of a Gaussian pump beam and Gaussian target spatial mode ; this might not be the case in other circumstances.

In order to find the focusing parameter ξ that gives rise to the highest collected brightness $K_2^{\rm opt}/(k_{p_0}L)$, we have performed optimizations similar to that of Fig. 3 for values of ξ ranging from 0.03 to 40, that is for waist radiuses from ~ 200 to ~ 5 μm for a red pump in common crystals, for instance. Knowing that $\zeta = 0$ is optimal in the whole range, we have plotted in Fig. 4 the values $K_2^{\rm opt}/(k_{p_0}L)$ (4a), $\alpha^{\rm opt}$ (4b) and ${\varphi_0}^{\rm opt}$ (4c) as a function of ξ.

According to Fig. 4b, the optimal normalized target mode waist $\alpha^{\rm opt}$ does not vary very much over this large range of focusing parameters. Starting with an approximate matching of the target mode to the pump waists $\alpha^{\rm opt} \approx 1$ at low focusing, our calculations exhibit a slow increase, showing that when focusing gets stronger, it is preferable to collect the weakly divergent photon pairs, since modes of larger waist sizes have smaller numerical apertures. On Fig. 4c, the optimum longitudinal phase mismatch ${\varphi_0}^{\rm opt}$ increases with the focusing parameter, as if to compensate for the transverse mismatch caused by the strong focusing.

Fig. 4a shows that the value of the focusing parameter giving the highest value of $K_2^{\rm opt}/(k_{p_0}L)$ is $\xi = 2.84$, for which the longitudinal phase mismatch is $\varphi_0 = 3.2$. These values correspond to the Boyd and Kleinman con-

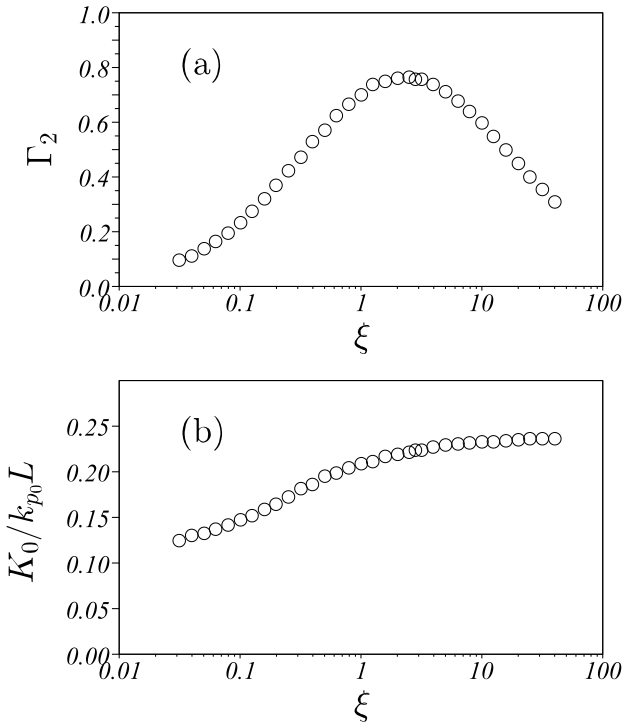

Fig. 5. Pair coupling efficiency $\Gamma_2 = P_2/\langle\psi_0|\psi_0\rangle$ (a) compared to the pair production probability (b), for various values of the focusing parameter ξ. P_0 is evaluated for the longitunal phase mismatch φ_0 that maximizes Γ_2.

ditions [48] for a highest second harmonic generation efficiency with Gaussian beams. Indeed, when evaluating the brightness produced in a single Gaussian mode, the collinear degenerate down-conversion is a process symmetric to second harmonic generation.

However, part of the down-converted photons are not in this particular target mode : Fig. 5a shows the ratio Γ_2 of the coupled brightness P_2 to the probability $P_0 = \langle\psi_0|\psi_0\rangle$, defined in section 2 B, of producing a photon pair within the filter bandwidth independently of its spatial coupling. Not only does Γ_2 not reach 1, but its optimum is slightly shifted from 2.84 to ~ 2. This is due to the variation of P_0 with ξ as depicted in Fig. 5b. For a red pump in common crystals, this shift in ξ corresponds to a waist radius difference of about 20 % but the shift may be more significant with different filtering or crystal configurations. However, it is to be noted that maximizing Γ_2 rather than P_2 has no practical advantage apart from a higher power efficiency.

D. *Optimization of the conditional coupling efficiency*

The conditional coupling efficiency $\Gamma_{2|1}$ (Eq. (36)) requires the computation of the single-photon coupling probability P_1, (cf. Eq. (32)):

$$P_1 = \frac{\mathscr{E}_p \chi_{\text{eff}}^2 L \Delta\omega_{\text{F}} \omega_{s_0}\omega_{i_0}\omega_{p_0}}{8\epsilon_0 c^4 n_s n_i} \cdot \frac{\Omega_1}{\Delta\omega_{\text{F}}}(\delta) \cdot \frac{K_1}{k_{p_0}L}(\xi,\alpha,\zeta,\varphi_0) \tag{52}$$

where $\frac{\Omega_1}{\Delta\omega_{\text{F}}}$ only depends on the shape of the filter itself and where

$$\frac{K_1}{k_{p_0}L} = \frac{4}{\pi^4}\xi\alpha^2 \iint d^2\boldsymbol{\varphi}_s \left| \iint d^2\boldsymbol{\varphi}_i Q_1 \right|^2 \tag{53}$$

with

$$\begin{aligned} Q_1 = &\exp\Big\{ -|\boldsymbol{\varphi}_s + \boldsymbol{\varphi}_i|^2 \Big\} \\ &\times \exp\Big\{ -\alpha^2 |\boldsymbol{\varphi}_s|^2 \Big\} \\ &\times \exp\ \mathrm{i}\Big\{ -4\xi\zeta \frac{n_p}{n_s'} |\boldsymbol{\varphi}_s|^2 \Big\} \\ &\times \operatorname{sinc}\left\{ \frac{\varphi_0}{2} - \xi\Big[|\boldsymbol{\varphi}_s + \boldsymbol{\varphi}_i|^2 - 2\frac{n_p}{n_s}|\boldsymbol{\varphi}_s|^2 - 2\frac{n_p}{n_i}|\boldsymbol{\varphi}_i|^2 \Big] \right\} \end{aligned} \tag{54}$$

which can be reduced to a 3D-integral as for Q_2 and Q_0.

The conditional coupling efficiency $\Gamma_{2|1} = K_2/K_1$ is plotted in Fig. 6 as a function of parameters α and φ_0 for three values of the focusing parameter $\xi = 0.1, 1, 10$. Contrary to the coupled brightness (whose variation with ξ can be seen in Fig. 4a through the spatial filtering factor $K_2/(k_{p_0}L)$), the conditional coupling efficiency can reach a value close to its maximum on the whole range of ξ. A large range of φ_0 is compatible with this maximum, but its overlap with the range leading to a high brightness is small. On the contrary, the tolerance on α is relatively low. When the results of P_2 and $\Gamma_{2|1}$ are both taken into account, the theory gives indeed useful information about the target mode waist for which the collection should be optimized with respect to the longitudinal phase mismatch parameter φ_0 (through the crystal temperature in the case of periodically poled crystals for instance), to find the best compromise between the coupled brightness and the conditional coupling efficiency.

The details of an experiment that enabled a validation of our model is given in the following section.

4. Experimental validation

A. *Experimental setup*

The experimental setup used to validate the theory is depicted in Fig. 7. SPDC is generated by focusing a pulsed pump beam at 782 nm in a periodically poled lithium niobate (PPLN) crystal of length $L = 2$ cm with a poling period $\Lambda = 19.34\mu$m. A "type 0" phase matching (pump, signal and idler have identical polarizations) has been chosen. The mean pump power is 5 mW and the 25 ns Gaussian pulses (FWHM) are Fourier transform limited with a 2 MHz repetition rate. The spatial profile of the pump beam is also Gaussian. On-axis fluorescence around 1564 nm is collected into a telecom optical fiber through the lenses L_c (achromatic doublet) and L_i (asphere). The same low bandwidth filter

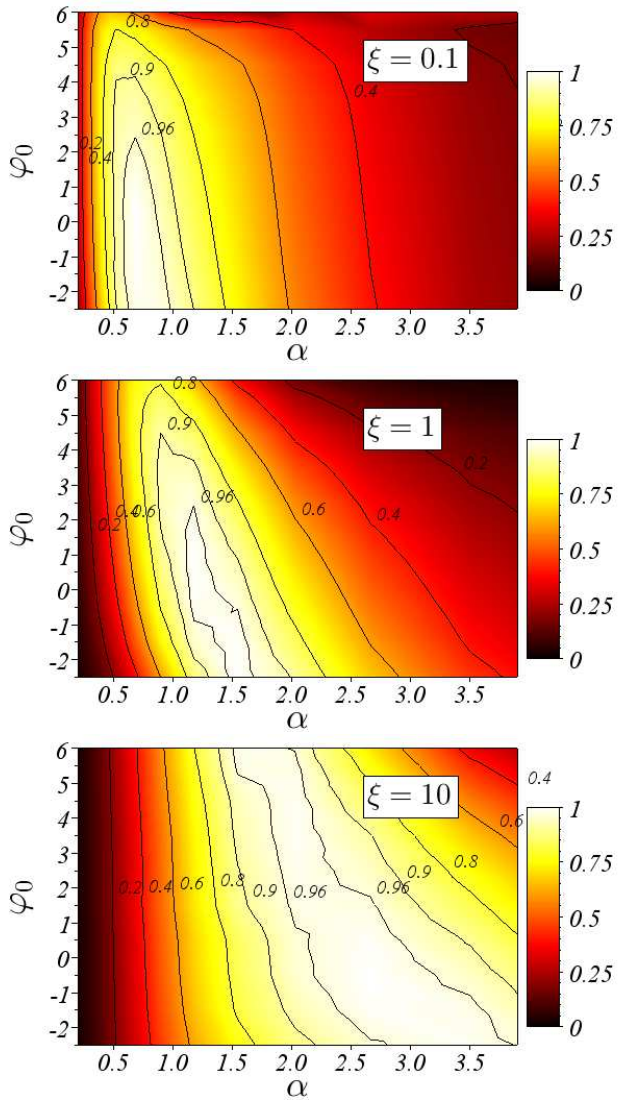

Fig. 6. Optimization of the conditional coupling efficiency $\Gamma_{2|1}$ with respect to the normalized target mode waist α and the longitudinal phase mismatch φ_0 for three values of the focusing parameter ξ: (a) $\xi = 0.1$, (b) $\xi = 1$, (c) $\xi = 10$.

($\Delta\omega_F = 2\pi \times 75$ GHz) is used for both signal and idler photons so that the source is operated at the degeneracy frequency ($\omega_{s_0} = \omega_{i_0} = \omega_{p_0}/2$). A balanced coupler is used to split photon pairs with 50 % efficiency and the photons are detected on paths A and B.

B. *Experimental method*

In order to explain how the conditional coupling efficiency $\Gamma_{2|1}$ can be determined experimentally, let us show its relation to measured parameters.

$$\Gamma_{2|1} = \frac{K_2}{K_1} = \frac{\Omega_1}{\Omega_2}\frac{P_2}{P_1}. \tag{55}$$

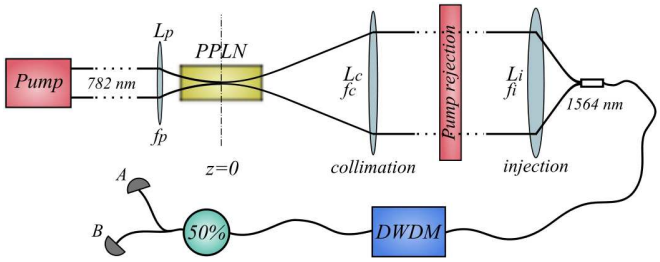

Fig. 7. Experimental setup: A pulsed pump laser at wavelength 782 nm is focused in a periodically-poled lithium niobate crystal (PPLN) with a lens L_p of focal length f_p. Down-converted photons at 1564 nm are coupled into an single mode fiber through an optical system composed of lenses L_c and L_i of respective focal lengths f_c and f_i. Spectral filtering is performed via a DWDM add-drop filter of bandwidth 75 GHz, and photons are split with 50 % efficiency towards detectors A and B using a balanced fibered coupler.

The experimental parameter corresponding to the calculated P_2 (Eq.42) is $P_{\rm AB}$, the measured coincidence probability per pulse from which accidental and noise coincidences are subtracted, and P_I is related to the measured counts on channel $I = A, B$ from which dark counts have been subtracted:

$$P_{\rm AB} = \mathcal{T}_{\rm A}\mathcal{T}_{\rm B}P_2 \qquad P_I = \mathcal{T}_I P_1 \tag{56}$$

where $\mathcal{T}_I$ is the transmission factor on channel I including the 50% loss induced by the coupler. We obtain

$$\Gamma_{2|1} = \frac{\Omega_1}{\Omega_2}\frac{\mathcal{T}_I}{\mathcal{T}_{\rm A}\mathcal{T}_{\rm B}}\frac{P_{\rm AB}}{P_I}. \tag{57}$$

The conditional coupling efficiency $\Gamma_{2|1}$ can hence be determined from the measurements of single counts and coincidences, provided the transmission factors have been previously determined. $\mathcal{T}_I$ is measured by injecting a narrowband laser at frequency $\omega_p/2$ in the fiber output where the photon detector is otherwise connected, and measuring the transmitted power on a detector positioned right after the crystal [46]. It is also necessary to measure the filter shape by tuning the frequency of the narrowband laser in the whole filter bandwidth, so that Ω_1 and Ω_2 can be determined. It is then possible to validate the dependence of $\Gamma_{2|1}$ with respect to the pump focusing parameter ξ and the normalized target mode waist α.

The variation of ξ was obtained by changing the lens L_p focusing the pump beam into the PPLN crystal. For each value of the focal length f_p, the waist of the pump beam was measured, allowing the determination of z_R and $\xi = L/(2z_R)$.

Counts and coincidences were then measured using various focal lengths f_i of the lens focusing the SPDC beam into the fiber. The value a_0 of the image of the fiber waist in the crystal was determined using the magnification factor f_c/f_i of the collection system (composed

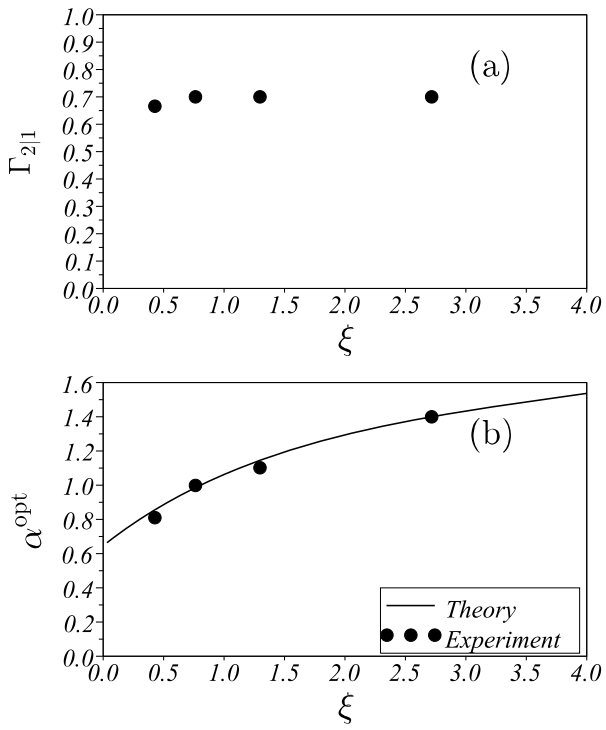

Fig. 8. (a) Measured conditional coupling efficiency $\Gamma_{2|1}$ plotted for four focal lengths $f_p = 150, 100, 75, 50$ mm, as a function of the focusing parameter $\xi = 0.44, 0.76, 1.05, 2.70$. (b) Corresponding experimental (circles) and calculated (solid line) values of the normalized target mode waist α for each value of $\Gamma_{2|1}$

.

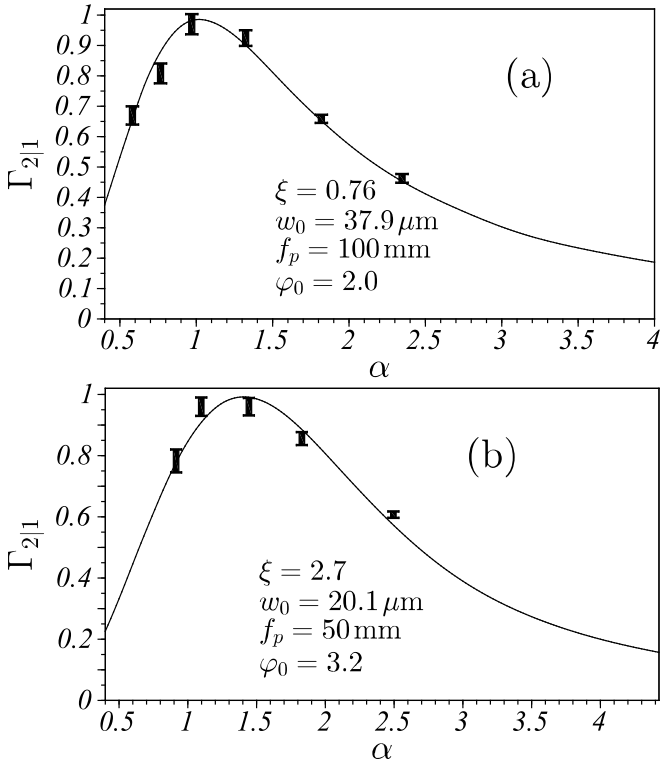

Fig. 9. Conditional coupling efficiency $\Gamma_{2|1}$: experimental values normalized to the measured maximum (represented with their error bars) and theoretical values (solid line), plotted as a function of the normalized target mode waist α, for two different focusing parameters: $\xi = 0.76$ (a) and $\xi = 2.7$ (b). The corresponding raw data are given in Appendix B.

of the lenses L_c and L_i) in order to determine $\alpha = a_0/w_0$. Let us note that each data point requires changing the focusing lens, realigning the setup, and successively optimizing the collection with at least five different injection lenses, with the phase mismatch (crystal temperature) as an additional degree of freedom.

C. *Experimental results*

The conditional coupling efficiency was derived using the measurements of $\mathcal{T}_{\rm A} = 0.026$ and $\mathcal{T}_{\rm B} = 0.024$. In Fig. 8a, the measured conditional coupling efficiency $\Gamma_{2|1}$ is plotted as a function of the focusing parameter ξ. The result is almost constant, as predicted by the theory, but around 30 % below the expected optimal value that is close to 100 %. This difference is probably due to imperfections in the Gaussian pump beam and aberrations in the optical system used to eliminate pump photons and to collect down-converted photon pairs into the fiber. The values of the normalized target mode waist α as a function of ξ for each value of $\Gamma_{2|1}$ are shown in Fig. 8b.

The variation of the measured value of $\Gamma_{2|1}$ with the normalized target mode waist α can then be compared to the theoretical predictions. Figure 9 shows two examples: the pump focusing is kept constant with $f_p = 100$ mm ($\xi = 0.76$, Fig. 9a) or $f_p = 50$ mm ($\xi = 2.7$, Fig. 9b). The experimental value of $\Gamma_{2|1}$ is normalized to the maximum of Fig. 8a and plotted as a function of α for $\zeta = 0$ while the appropriate value of the remaining unknown dimensionless parameter φ_0 is found by horizontally fitting the theoretical curve to the experimental data. For $\xi = 0.76$, φ_0 is found to be around 2.0 while it is around 3.2 for $\xi = 2.7$. These values of φ_0 are also in agreement with the theoretical predictions corresponding to the coupled brightness optimization. Indeed, although each plotted value of $\Gamma_{2|1}$ was obtained after optimizing this figure of merit itself, the experimental starting point was a preliminary optimization around a maximum coupled brightness. As $\Gamma_{2|1}$ and P_2 have a common optimum in the (α, φ_0) space, it is not surprising to converge close to $(\alpha^{\rm opt}, {\varphi_0}^{\rm opt})$ (optimum of P_2 as shown in Fig. 4 as a function of ξ) when optimizing with respect to $\Gamma_{2|1}$.

The very good agreement of our theory with the experimental results confirms its validity. Using our analysis for practical applications, only the measurement of the pump waist is required in order to determine the optimum value of α and hence the lens system that couples the down-converted photons into the most appropriate

single mode. The phase-matching parameter φ_0 (i.e. in our case, the crystal temperature) is the only remaining degree of freedom and has to be optimized experimentally.

In summary, we have confirmed experimentally 1) the quasi-independence of the conditional coupling efficiency on the focusing parameter, 2) its dependence on the target mode size and 3) that our theory predicts with a very good precision the optimal target mode waist size for a particular focusing parameter.

5. Discussion

A. *Comparison with other works*

As mentioned in the introduction, our work covers issues that were addressed by other authors with various assumptions or methods. Both the absolute coupled brightness and the conditional coupling efficiency can provide a relevant comparison. We will also discuss a few reported experimental validations.

About the brightness, Ling *et al.* [37] were among the first to propose an expression of the absolute photon pair rate collected into a single Gaussian spatial mode. Apart from the fact that they consider the case of a continuous pump ($\delta = 0$), our calculations are consistent dimension-wise. Moreover, after identifying in their analysis a spatial filtering factor analogous to our $K_2/(k_{p_0}L)$, we found it to be proportional to $\sim \xi\,\mathrm{sinc}^2(\varphi_0/2)$. This is indeed the result we find for the specific case of low focusing ($\xi \ll 1$) and $\alpha = \sqrt{2}$, which correspond to Ling's assumptions: thin crystal, negligible pump diffraction, equal Rayleigh lengths for pump and down-converted photons. However, under our less restrictive assumptions, we have shown that $\alpha = \sqrt{2}$ is optimal for $\xi = 2.84$, whereas for low focusing, $\alpha \leq 1$.

More recently, the absolute value of the coupled brightness was calculated by Mitchell [38] in the Heisenberg picture, under assumptions similar to ours. This investigation has been restricted to a monochromatic, continuous pump field, and a direct expansion of the Hamiltonian onto the target Gaussian modes has been performed, as opposed to our choice of investigating the single-mode coupling of free-space expanded fluorescence. Our theory, which is developed in the Schrödinger picture, is nevertheless fully consistent with the results of Mitchell and we suggest in the next subsection how to generalize it using the same framework.

As for the dependence on crystal length, our results concerning the pair collection efficiency are consistent with that of Bennink [39], who found a linear dependence when the source bandwidth is much smaller than the phase-matching bandwidth, as opposed to Ljunggren *et al.* [36] who conclude on a $\sqrt{L}$-dependence. Let us point out that, as Bennink [39], we have taken into account the diffracting nature of the pump beam, and considered the longitudinal phase mismatch as a degree of freedom for optimization. As a result, our optimization of P_2 for Gaussian beams at the degenerate frequency is optimal close to the well-known Boyd & Kleinman conditions [48]: $\xi = 2.84$, $\varphi_0 = 3.2$ and equal Rayleigh length for the pump and down-converted photons ($\alpha = \sqrt{2}$). An advantage of our framework is that the particular pump and target modes, filter shape, pump linewidth, etc. are only used in the very last step of the optimization, *i.e.* the computation of a multiple integral. Up to then, our framework remains very general.

As far as the conditional coupling efficiency is concerned, contrary to the coupled brightness, it is found to be close to 1 for any focusing strength, provided the target mode waist α and phase mismatch φ_0 are adjusted according to our theory. Interestingly, a subset of (α, φ_0) which maximizes the conditional coupling efficiency is generally close to the optimal brightness, giving the configuration for an optimal general source performance. Benninck [39] finds, on the other hand, that a strong reduction of brightness is necessary to achieve a high heralding ratio, highlighting what could be a fundamental trade-off for single-mode applications. The results may however be consistent when we consider the narrow-band assumption under which our optimization is valid.

As remarked by Bennink, very few among the reported theoretical works have been experimentally validated, probably because of the complexity of such experiments that involve multiple parameters to optimize simultaneously and to measure precisely. Reported experiments were realized for a single set of non-optimal parameters [36] or in a configuration which is not in the scope of our theory [35]. We showed that our model could be used in order to optimize the experimental source configuration.

B. *Extension to other source designs*

Although the calculation done in section 3 uses a bulk periodically-poled crystal pumped with a single-mode diffractive Gaussian pump beam, as required for successful comparison with our experiment, the general theoretical framework of section 2 can be applied to other source designs. A few examples are given hereafter.

Let us start with the question of phase-matching. Our model is perfectly suited for the quasi-phase matching case, where pump, signal and idler have identical polarization. Type I phase matching can also be described correctly, although one should take into account the decrease of the interaction length due to walk-off. Type II phase-matching involves different target modes for signal and idler photons, which is not taken into account here.

As far as the crystal type is concerned, a non-periodically or multi-periodically poled crystal can be used by coherently summing the first N components of the Fourier series expansion of the nonlinear susceptibility $\overline{\overline{\chi}}^{(2)}(z)$. When $\overline{\overline{\chi}}^{(2)}(z)$ is not of high complexity, the expansion can be truncated to a low N, making the calculation not much more time-consuming.

The theory developed here is still valid in the case of a monochromatic pump, provided the coincidences are

evaluated within a given time window and the pump pulse energy $\mathcal{E}_p$ is replaced by the pump power multiplied by this time window.

It is quite straightforward to correct the results for non-degenerate down conversion, provided the frequency difference is small compared to the pump frequency.

It is also possible to use a non-Gaussian pump or target mode profile, by changing the functions S_p and $\mathcal{O}_0$ respectively. If required, a second dimensionless parameter must be introduced apart from α in order to characterize the mode ellipticity. In this case, the 4D- to 3D-integral reduction used in Eq. (50) is impossible due to the absence of cylindrical symmetry, making the computation longer. Let us note that for such high-dimensions integrals, a Monte-Carlo integration method could give faster results.

6. Conclusion

In this paper, we have calculated the state of a photon pair produced by a narrow-band spontaneous parametric down-conversion (SPDC) source with arbitrary pump spatial and temporal profile, and arbitrary filtering configuration.

When applied to Gaussian modes, our theory is consistent with the most recently reported works where realistic assumptions have been made. Within our assumptions, no incompatibility is observed between a high coupled brightness and a high conditional coupling efficiency, and thus a high heralding ratio in the narrow-band limit. We believe this result shows that SPDC sources are suitable for narrow-band quantum information applications.

The theoretical predictions about the matching between the pump focusing parameter and the target mode of down-conversion were found to be experimentally accurate. Knowing the optimal pump focusing parameter for a given target mode also defines which mode should be enhanced by a cavity so as to maximize both the coupled brightness and the conditional coupling efficiency. In this way, we can obtain an absolute optimum for a given crystal, which may be useful for designing cavity-enhanced SPDC sources [51].

Once validated under the Gaussian assumptions, our theoretical framework, which allows an extensive study of the source through many degrees of freedom, may be used to enable predicting the best performance for more original source designs, including non-Gaussian or non-fundamental Gaussian pump modes [52, 53], guided or diffractive, single or multi-mode, with arbitrary nonlinear susceptibility longitudinal distribution.

Acknowledgments

This work is a part of the project "embryonic Quantum Network", funded by the "Agence Nationale de la Recherche".

Appendix A: Filtering in the Schrödinger picture

In this appendix we describe the effect of spatial filters on a single photon state. Generalization to the case of photon pairs is made in Section 2 B.

1. *"Localized" photonic states and pseudo-wavefunction*

In this work, we use localized photonic states introduced by L. Mandel [49]. Based on plane-wave states $|1_{\mathbf{k}}\rangle$ in a quantization volume $\mathcal{V}$, a state describing a photon localized around $\mathbf{r}$ is defined by

$$|1_{\mathbf{r}}\rangle = \sum_{\mathbf{k}} \frac{e^{-i\mathbf{k}\cdot\mathbf{r}}}{\sqrt{\mathcal{V}}} |1_{\mathbf{k}}\rangle. \tag{A1}$$

Then, a general photon state $|\psi\rangle = \sum_{\mathbf{k}} \psi_{\mathbf{k}} |1_{\mathbf{k}}\rangle$ can be written as

$$|\psi\rangle = \int_{\mathcal{V}} d^3\mathbf{r}\, \psi(\mathbf{r}) |1_{\mathbf{r}}\rangle \tag{A2}$$

where $\psi(\mathbf{r})$ is a spatial pseudo-wavefunction for which $\psi_{\mathbf{k}}$ are the coefficients of its Fourier series expansion in the quantization volume $\mathcal{V}$. Such a wavefunction is only valid provided the volume V in which the localization probability $P(V)$, defined as follows, is evaluated is large enough (each dimension much larger that the wavelength):

$$P(V) = \int_V d^3\mathbf{r}\ |\langle 1_{\mathbf{r}}|\psi\rangle|^2 = \int_V d^3\mathbf{r}\ |\psi(\mathbf{r})|^2 \tag{A3}$$

This probability is naturally equal to unity in the quantization volume:

$$P(\mathcal{V}) = \int_{\mathcal{V}} d^3\mathbf{r}\ |\psi(\mathbf{r})|^2 = \langle\psi|\psi\rangle = \sum_{\mathbf{k}} |\psi_{\mathbf{k}}|^2 = 1. \tag{A4}$$

2. *Spatial filtering*

a. *Principle*

A spatial filter located on the propagation axis at $z = z_0$ is modeled as the coupling in the plane $z = z_0$ of the down-converted field into a single spatial mode defined by a function $\mathcal{O}_{\omega,0}(\mathbf{r})$. The index ω indicates that this spatial mode can be frequency-dependent for a given filter.

Note that z_0 may be in $[-L/2, L/2]$. As an example, if the spatial filtering is done via an optical fiber, the effective location of the filter is where the lens collection system images the entrance of the fiber.

To evaluate its transmitted component, the down-converted field initially described as a superposition of plane waves is better expanded on a particular set of orthogonal modes $\{\mathcal{O}_{\omega,j}(\mathbf{r})\}$, one of which $(\mathcal{O}_{\omega,0}(\mathbf{r}))$ being the spatial mode selected by the considered filter.

If coupled to other modes, photons are supposed to be lost. As for spectral filtering, this leads to a mixed state.

For instance, the fundamental mode can be the Gaussian mode of the Laguerre-Gauss basis, suited to single-mode fibers. Then $\mathcal{O}_{\omega,j=0}(\mathbf{r})$ describes a Gaussian beam

of waist size equal to the field radius of a fiber mode. If the image of the fiber entrance is located at $z = z_0$, $\mathcal{O}_{\omega,j=0}(\boldsymbol{\rho}, z_0)$ describes the Gaussian beam waist profile corresponding to the fiber transverse mode.

A projection at $z = z_0$ into that single mode selects the photon state component which is transmitted by the filter. Once transmitted, the state is said to be in the spatial mode characterized by the annihilation operator $\hat{o}_\omega$. Let us note that whether the spatial mode for $z \geq z_0$ continues to be that of a Gaussian beam (as for a cavity) or is actually described by a guided propagation with a constant transverse profile $\mathcal{O}_{\omega,0}(\boldsymbol{\rho}, z_0)$ and propagation constant $\beta_\omega = n'(\omega)\omega/c$ like in a single mode fiber of effective refractive index n' [50] will not change the description:

$$\mathcal{O}_{\omega,j=0}(\boldsymbol{\rho}, z \geq z_0) = \mathcal{O}_{\omega,0}(\boldsymbol{\rho}, z_0) e^{\mathrm{i}\beta_\omega (z-z_0)}. \tag{A5}$$

In a quantization volume $\mathcal{V} = \mathcal{S} \times \mathcal{L}$, a field in the mode $\mathcal{O}_{\omega,j}(\mathbf{r})$ will be said to be in the quantum state

$$|\mathcal{O}_{\omega,j}\rangle = \frac{1}{\sqrt{\mathcal{L}}} \int d^3\mathbf{r}\, \mathcal{O}_{\omega,j}(\mathbf{r}) |1_\mathbf{r}\rangle \tag{A6}$$

so that the states are normalized: $\langle \mathcal{O}_{\omega,j} | \mathcal{O}_{\omega,j'} \rangle = \delta_{jj'}$. Functions $\mathcal{O}_{\omega,j}(\mathbf{r})$ are only transversally normalized: $\int d^2\boldsymbol{\rho}\, \mathcal{O}^*_{\omega,j'}(\boldsymbol{\rho}, z) \mathcal{O}_{\omega,j}(\boldsymbol{\rho}, z) = \delta_{jj'}$ and $\int_\mathcal{V} d^3\mathbf{r}\, \mathcal{O}^*_{\omega,j'}(\mathbf{r}) \mathcal{O}_{\omega,j}(\mathbf{r}) = \mathcal{L}\, \delta_{jj'}$.

b. Calculation of the transmitted field component

In a quantization volume containing a crystal before $z = z_0$ and a spatial filter at z_0, a one-photon field in mode ℓ is in the state

$$\begin{aligned} |1_\ell\rangle &= \int d^3\mathbf{r}\, f(\mathbf{r}) |1_\mathbf{r}\rangle \qquad\qquad (A7) \\ &= \int d^3\mathbf{r} \left(\Theta(z_0 - z) \frac{e^{\mathrm{i}\mathbf{k}_\ell \cdot \mathbf{r}}}{\sqrt{\mathcal{V}}} \right. \\ &\left. + \Theta(z - z_0) \sum_j g_j(\ell) \frac{\mathcal{O}_{\omega_\ell,j}(\mathbf{r})}{\sqrt{\mathcal{L}}} \right) |1_\mathbf{r}\rangle \qquad\qquad (A8) \end{aligned}$$

where $\Theta(z)$ is Heaviside's function and $g_j(\ell)$ are determined by the boundary conditions at $z = z_0$:

$$\sum_j g_j(\ell) \frac{\mathcal{O}_{\omega_\ell,j}(\boldsymbol{\rho}, z_0)}{\sqrt{\mathcal{L}}} = \frac{e^{\mathrm{i}\boldsymbol{\kappa}'_\ell \cdot \boldsymbol{\rho}} e^{\mathrm{i}k'_{z,\ell} \cdot z_0}}{\sqrt{\mathcal{V}}}. \tag{A9}$$

Remark that the wavevector takes into account the change of medium according to Snell-Descartes' law of refraction:

$$\frac{\boldsymbol{\kappa}'}{\boldsymbol{\kappa}} = \frac{|\mathbf{k}'| \sin\theta'}{|\mathbf{k}| \sin\theta} = 1 \qquad \frac{k'_z}{k_z} = \frac{|\mathbf{k}'| \cos\theta'}{|\mathbf{k}| \cos\theta} \approx \frac{n'}{n} \tag{A10}$$

where n' is the refractive index of the medium in which $\mathcal{O}_{\omega_\ell,j}(\mathbf{r})$ describes the spatial mode and n the refractive index in the crystal.

Using the orthonormality of functions $\{\mathcal{O}_{\omega,j}(\mathbf{r})\}$, one gets

$$\begin{aligned} g_j(\ell) &= \int d^2\boldsymbol{\rho}\, \mathcal{O}^*_{\omega_\ell,j}(\boldsymbol{\rho}, z_0) \frac{e^{\mathrm{i}\boldsymbol{\kappa}_\ell \cdot \boldsymbol{\rho}} e^{\mathrm{i}k'_{z,\ell} \cdot z_0}}{\sqrt{\mathcal{V}}} \sqrt{\mathcal{L}} \\ &= \frac{1}{\sqrt{\mathcal{S}}} e^{\mathrm{i}k'_{z,\ell} \cdot z_0} \breve{\mathcal{O}}^*_{\omega_\ell,j}(\boldsymbol{\kappa}_\ell, z_0) \end{aligned} \tag{A11}$$

where $\breve{\mathcal{O}}_{\omega_\ell,j}(\boldsymbol{\kappa}, z_0)$ is the Fourier transform of $\mathcal{O}_{\omega_\ell,j}(\boldsymbol{\rho}, z_0)$ and * designates a complex conjugate.

Starting from an initial state $|\Psi(t_0)\rangle = \sum_\ell \mu_\ell |1_\ell\rangle$ localized at $z < z_0$, the state becomes for $z > z_0$

$$|\Psi(t_1)\rangle = \sum_j \sum_\ell \mu_\ell e^{\mathrm{i}k'_{z,\ell} \cdot z_0} \frac{1}{\sqrt{\mathcal{S}}} \breve{\mathcal{O}}^*_{\omega_\ell,j}(\boldsymbol{\kappa}_\ell, z_0) |\mathcal{O}_{\omega_\ell,j}\rangle. \tag{A12}$$

Ignoring components of the state which are not within the mode $|\mathcal{O}_{\omega_\ell,0}\rangle$ transmitted by the filter, the transmitted one-photon state becomes:

$$\begin{aligned} |\Psi(t_1)\rangle = \sum_\ell \mu_\ell e^{\mathrm{i}k'_{z,\ell} \cdot z_0} \frac{1}{\sqrt{\mathcal{S}}} \breve{\mathcal{O}}^*_{\omega_\ell,0}(\boldsymbol{\kappa}_\ell, z_0) |\mathcal{O}_{\omega_\ell,0}\rangle \\ \oplus \textit{ ignored zero-photon terms.} \end{aligned} \tag{A13}$$

The sign $\oplus$ means an incoherent sum, ie where no interference is possible between its terms (statistical mixture).

Note that if one of the functions $\{\mathcal{O}_{\omega,j}(\mathbf{r})\}$ describes the spatial eigenmode of any other filter (*e.g.* a rectangular waveguide), the result is still valid.

This method is extended to two-photon states in the rest of the paper.

Appendix B: Examples of experimental data

Table 1 gives the experimental data corresponding to Fig. 9a ($f_p = 100$ mm) and b ($f_p = 50$ mm). The single count probabilities have been obtained by dividing the counts per second by the effective pump trigger rate (detector dead time of 10 μs taken into account). The true coincidence probability P_{AB} was obtained by subtracting the accidental and noise coincidence probabilities from the total coincidence probability [46]. The dark count figures on detector A and B were respectively $P_{NA} = 1.9 \times 10^{-4}$ and $P_{NB} = 1.5 \times 10^{-4}$ and the ratio $\Omega_1/\Omega_2 = 1.14$.

For each value of the focal length f_i, three or more data points are given, corresponding to different pump power values.

In section 4, the value of $\Gamma_{2|1}$ is derived using Eq. 57.

References

1. W. Tittel and G. Weihs, "Photonic entanglement for fundamental tests and quantum communication," Quantum Information and Computation **1**, 3–56 (2001).

Table 1. Raw single counts (N_A, N_B) and coincidences (N_C) per second, net single count probabilities (P_A, P_B) and true coincidence probability P_{AB}. Values in Hz are the result of averaging for around 1 min.

Used in Fig. 9a.

f_i (mm)	N_A (Hz)	N_B (Hz)	N_C (Hz)	P_A $\times 10^{-3}$	P_B $\times 10^{-3}$	P_{AB} $\times 10^{-5}$
	2681	2653	20.12	1.18	1.20	0.85
6.2	4281	4269	38.66	2.03	2.06	1.52
	6155	6131	60.27	3.07	3.09	2.15
	2563	2544	25.98	1.12	1.14	1.16
8	3222	3197	34.91	1.46	1.48	1.53
	5967	5925	74.47	2.97	2.98	2.97
	3255	3239	48.21	1.48	1.51	2.21
	5700	5685	92.87	2.82	2.84	4.02
11	2099	2065	27.38	0.87	0.89	1.29
	5405	5395	85.47	2.65	2.68	3.71
	3050	3027	44.18	1.37	1.39	2.03
	1505	1460	16.77	0.57	0.58	0.80
	1794	1750	23.48	0.71	0.73	1.11
15	4152	4123	65.72	1.96	1.98	2.97
	4267	4237	69.59	2.02	2.04	3.15
	6373	6340	107.20	3.20	3.21	4.58
	2817	2781	35.72	1.25	1.26	1.63
19	4528	4491	63.51	2.17	2.18	2.77
	6367	6336	92.81	3.19	3.21	3.81
	2678	2637	28.78	1.18	1.19	1.29
25	4162	4132	48.14	1.97	1.99	2.05
	5693	5653	69.61	2.81	2.83	2.79

Used in Fig. 9b.

f_i (mm)	N_A (Hz)	N_B (Hz)	N_C (Hz)	P_A $\times 10^{-3}$	P_B $\times 10^{-3}$	P_{AB} $\times 10^{-5}$
	5496	5296	64.00	2.70	2.64	2.58
11	4196	4030	45.77	1.99	1.94	1.93
	3068	2934	30.48	1.38	1.35	1.33
	6085	5868	94.15	3.03	2.95	4.01
15	4023	3868	58.11	1.90	1.85	2.61
	1986	1888	23.98	0.82	0.81	1.13
	6431	6227	111.24	3.23	3.16	4.81
19	4096	3951	64.47	1.93	1.90	2.92
	2063	1964	28.54	0.86	0.85	1.35
	6131	5947	103.93	3.06	3.00	4.51
25	5133	4961	86.29	2.50	2.45	3.85
	3082	2965	47.06	1.39	1.37	2.19
	6537	6299	95.01	3.29	3.20	3.92
30	4883	4704	66.93	2.36	2.31	2.89
	3126	3006	40.91	1.41	1.39	1.86

2. S. Gröblacher, T. Paterek, R. Kaltenbaek *et al.*, "An experimental test of non-local realism," Nature **446**, 871–875 (2007).
3. N. Gisin and R. Thew, "Quantum communication," Nature Photonics **1**, 165–171 (2007). 10.1038/nphoton.2007.22.
4. N. Gisin and R. T. Thew, "Quantum communication technology," Electronics Letters **46**, 965–U20 (2010).
5. A. K. Ekert, "Quantum cryptography based on Bell's theorem," Phys. Rev. Lett. **67**, 661–663 (1991).
6. J. H. Shapiro, "Architectures for long-distance quantum teleportation," New Journal of Physics **4**, 47 (2002).
7. C. Simon, H. de Riedmatten, M. Afzelius, N. Sangouard, H. Zbinden, and N. Gisin, "Quantum repeaters with photon pair sources and multi-mode memories," Phys. Rev. Lett. 98, 190503 (2007).
8. F. Wong, J. Shapiro, and T. Kim, "Efficient generation of polarization-entangled photons in a nonlinear crystal," Laser Physics **16**, 1517–1524 (2006).
9. P. G. Kwiat, K. Mattle, H. Weinfurter, A. Zeilinger, A. V. Sergienko, and Y. Shih, "New high-intensity source of polarization-entangled photon pairs," Phys. Rev. Lett. **75**, 4337–4341 (1995).
10. T. G. Noh, H. Kim, T. Zyung, and J. Kim, "Efficient source of high purity polarization-entangled photon pairs in the 1550 nm telecommunication band," Appl. Phys. Lett. **90**, 011116 (2007).
11. J. Altepeter, E. Jeffrey, and P. Kwiat, "Phase-compensated ultra-bright source of entangled photons," Opt. Express **13**, 8951–8959 (2005).
12. B. Shi and A. Tomita, "Highly efficient generation of pulsed photon pairs with bulk periodically poled potassium titanyl phosphate," J. Opt. Soc. Am. B **21**, 2081–2084 (2004).
13. H. Guillet de Chatellus, A. Sergienko, B. Saleh, M. Teich, and G. Di Giuseppe, "Non-collinear and non-degenerate polarization-entangled photon generation via concurrent type-I parametric downconversion in ppln," Opt. Express **14**, 10060–10072 (2006).
14. M. Fiorentino, C. Kuklewicz, and F. Wong, "Source of polarization entanglement in a single periodically poled KTiOPO4 crystal with overlapping emission cones," Opt. Express **13**, 127–135 (2005).
15. A. Fedrizzi, T. Herbst, A. Poppe, T. Jennewein, and A. Zeilinger, "A wavelength-tunable fiber-coupled source of narrowband entangled photons," Opt. Express **15**, 15377–15386 (2007).
16. O. Kuzucu and F. N. C. Wong, "Pulsed sagnac source of narrow-band polarization-entangled photons," Phys. Rev. A **77**, 032314 (2008).
17. S. Virally, S. Lacroix, and N. Godbout, "Limits of heralded single-photon sources based on parametric photon-pair generation," Phys. Rev. A **81**, 013808 (2010).
18. J. L. Smirr, R. Frey, E. Diamanti, R. Alléaume, and I. Zaquine, "Intrinsic limitations to the quality of pulsed spontaneous parametric downconversion sources for quantum information applications," J. Opt. Soc. Am. B **28**, 832–841 (2011).
19. A. Lvovsky, B. Sanders, and W. Tittel, "Optical quantum memory," Nature Photonics **3**, 706–714 (2009).
20. C. Simon, M. Afzelius, J. Appel, A. Boyer de la Giroday, S. J. Dewhurst, N. Gisin, C. Y. Hu, F. Jelezko, S. Kröll, J. H. Müller, J. Nunn,

E. S. Polzik, J. G. Rarity, H. De Riedmatten, W. Rosenfeld, A. J. Shields, N. Sköld, R. M. Stevenson, R. Thew, I. A. Walmsley, M. C. Weber, H. Weinfurter, J. Wrachtrup and R. J. Young, "Quantum memories," Eur. Phys. J. D **58**, 1–22 (2010).
21. T. Chanelière, J. Ruggiero, M. Bonarota, M. Afzelius, and J.-L. L. Gouët, "Efficient light storage in a crystal using an atomic frequency comb," New Journal of Physics **12**, 023025 (2010).
22. E. Saglamyurek, N. Sinclair, J. Jin, J. Slater, D. Oblak, F. Bussières, M. George, R. Ricken, W. Sohler, and W. Tittel, "Broadband waveguide quantum memory for entangled photons," Nature **469**, 512 (2011).
23. C. Clausen, I. Usmani, F. Bussières,N. Sangouard, M. Afzelius, H. de Riedmatten, N. Gisin, "Quantum storage of photonic entanglement in a crystal," Nature **469**, 508 (2011).
24. W. H. Louisell, A. Yariv, and A. E. Siegman, "Quantum fluctuations and noise in parametric processes," Phys. Rev. **124**, 1646–1654 (1961).
25. C. K. Hong and L. Mandel, "Theory of parametric frequency down conversion of light," Phys. Rev. A **31**, 2409–2418 (1985).
26. R. Ghosh and L. Mandel, "Observation of nonclassical effects in the interference of two photons," Phys. Rev. Lett. **59**, 1903–1905 (1987).
27. L. Mandel, "Quantum effects in one-photon and two-photon interference," Rev. Mod. Phys. **71**, S274–S282 (1999).
28. M. H. Rubin, D. N. Klyshko, Y. H. Shih, and A. V. Sergienko, "Theory of two-photon entanglement in type-II optical parametric down-conversion," Phys. Rev. A **50**, 5122–5133 (1994).
29. T. E. Keller and M. H. Rubin, "Theory of two-photon entanglement for spontaneous parametric down-conversion driven by a narrow pump pulse," Phys. Rev. A **56**, 1534–1541 (1997).
30. T. B. Pittman, D. V. Strekalov, D. N. Klyshko, M. H. Rubin, A. V. Sergienko, and Y. H. Shih, "Two-photon geometric optics," Phys. Rev. A **53**, 2804–2815 (1996).
31. A. Joobeur, B. E. A. Saleh, and M. C. Teich, "Spatio-temporal coherence properties of entangled light beams generated by parametric down-conversion," Phys. Rev. A **50**, 3349–3361 (1994).
32. C. Kurtsiefer, M. Oberparleiter, and H. Weinfurter, "High-efficiency entangled photon pair collection in type-II parametric fluorescence," Phys. Rev. A **64**, 023802 (2001).
33. F. A. Bovino, P. Varisco, A. M. Colla, G. Castagnoli, G. D. Giuseppe, and A. V. Sergienko, "Effective fiber-coupling of entangled photons for quantum communication," Optics Communications **227**, 343 – 348 (2003).
34. S. Castelletto, I. P. Degiovanni, A. Migdall, and M. Ware, "On the measurement of two-photon single-mode coupling efficiency in parametric down-conversion photon sources," New Journal of Physics **6**, 87 (2004).
35. S. Castelletto, I. Degiovanni, G. Furno, V. Schettini, A. Migdall, and M. Ware, "Two-photon mode preparation and matching efficiency: definition, measurement, and optimization," Instrumentation and Measurement, IEEE Transactions on **54**, 890–893 (2005).
36. D. Ljunggren and M. Tengner, "Optimal focusing for maximal collection of entangled narrow-band photon pairs into single-mode fibers," Phys. Rev. A **72**, 062301 (2005).
37. A. Ling, A. Lamas-Linares, and C. Kurtsiefer, "Absolute emission rates of spontaneous parametric down-conversion into single transverse gaussian modes," Phys. Rev. A **77**, 043834 (2008).
38. M. W. Mitchell, "Parametric down-conversion from a wave-equation approach: Geometry and absolute brightness," Phys. Rev. A **79**, 043835 (2009).
39. R. S. Bennink, "Optimal collinear gaussian beams for spontaneous parametric down-conversion," Phys. Rev. A **81**, 053805 (2010).
40. R. Boyd, *Nonlinear optics* (Academic Press, 2008).
41. A. Yariv, *Quantum electronics* (Wiley, 1989).
42. M. Fiorentino, G. Messin, C. E. Kuklewicz, F. N. C. Wong, and J. H. Shapiro, "Generation of ultrabright tunable polarization entanglement without spatial, spectral, or temporal constraints," Phys. Rev. A **69**, 041801 (2004).
43. M. Hentschel, H. Hübel, A. Poppe, and A. Zeilinger, "Three-color sagnac source of polarization-entangled photon pairs," Opt. Express **17**, 23153–23159 (2009).
44. J. Garrison and R. Chiao, *Quantum optics* (Oxford University Press, 2008).
45. J. Shapiro, "The quantum theory of optical communications," Selected Topics in Quantum Electronics, IEEE Journal of **15**, 1547 –1569 (2009).
46. J. L. Smirr, S. Guilbaud, J. Ghalbouni, R. Frey, E. Diamanti, R. Alléaume, and I. Zaquine, "Simple performance evaluation of pulsed spontaneous parametric down-conversion sources for quantum communications," Opt. Express **19**, 616–627 (2011).
47. J. Berntsen, T. O. Espelid, and A. Genz, "An adaptive algorithm for the approximate calculation of multiple integrals," ACM Trans. Math. Softw. **17**, 437–451 (1991).
48. G. D. Boyd and D. A. Kleinman, "Parametric interaction of focused gaussian light beams," J. Appl. Phys. **39**, 3597–3639 (1968).
49. L. Mandel, "Configuration-space photon number operators in quantum optics," Phys. Rev. **144**, 1071–1077 (1966).
50. A. Ghatak and K. Thyagarajan, *Introduction to fiber optics* (Cambridge University Press, 1998).
51. Y. Jeronimo-Moreno, S. Rodriguez-Benavides, and A. B. U'Ren, "Theory of Cavity-Enhanced Spontaneous Parametric Downconversion," Laser Phys. **20**,

1221–1233 (2010).
52. J. Romero, D. Giovannini, M. G. McLaren, E. J. Galvez, A. Forbes, and M. J. Padgett, "Orbital angular momentum correlations with a phase-flipped Gaussian mode pump beam," Journal of Optics **14**, 085401 (2012).
53. J. W. Kim, J. I. Mackenzie, J. R. Hayes, and W. A. Clarkson, "High-power fibre-laser-pumped Er:YAG laser with 'top-hat' output beam," 2011 Conference on Lasers and Electro-Optics Europe and 12th European Quantum Electronics Conference (CLEO EUROPE/EQEC), Munich, Germany, May 2011.